Schweizerischer Erdbebendienst
Service Sismologique Suisse
Servizio Sismico Svizzero
Swiss Seismological Service

ETH zürich

SITE CHARACTERIZATION REPORT

SKRK: Kreuzlingen (TG) - Kantonsschule

Manuel Hobiger, Donat Fäh

Last Modification: 25/02/2020

Schweizerischer Erdbebendienst (SED)
Service Sismologique Suisse
Servizio Sismico Svizzero
Servizi da Terratrembels Svizzer

ETH Zürich
Sonneggstrasse 5
8092 Zürich
Schweiz
manuel.hobiger@sed.ethz.ch

Contents

Summary

The free-field strong-motion station SKRK was built next to the Kantonsschule in Kreuzlingen (TG). We performed a passive seismic array measurement with two array configurations to characterize the soil underneath the station.
The measurements show that the fundamental frequency of the structure beneath the station is about 0.5-0.6 Hz and a second peak is found at around 3 Hz. The array measurements were analyzed with different techniques, namely 3-component HRFK, WaveDec and SPAC. All techniques gave similar dispersion curves. The dispersion curves for the fundamental modes of both Love and Rayleigh waves could be retrieved from around 2.7 to 19 Hz and 3.5 to 36.5 Hz, respectively.
The joint inversion of Love and Rayleigh wave dispersion curves and the Rayleigh wave ellipticity angle showed that the structure can be explained by models with interfaces at around 1.5 m, 14 m and 42 m depth. The V_{S30} of the best models is about 437 m/s, corresponding to soil class B in EC8 and C in SIA261.

1 Introduction

In the framework of the second phase of the Swiss Strong Motion Network (SSMNet) renewal project, a new station was planned in Kreuzlingen (TG).
The site selection resulted in the Kantonsschule as the best site in the area. The new station, called SKRK, went operational on 17 April 2015. The location of the station is shown in Fig. 1.

Figure 1: Map showing the location of station SKRK in Kreuzlingen.

2 Geological setting

A geological map of the surroundings of station SKRK is shown in Fig. 2. The station is located on agradation deposits of Lake Constance.

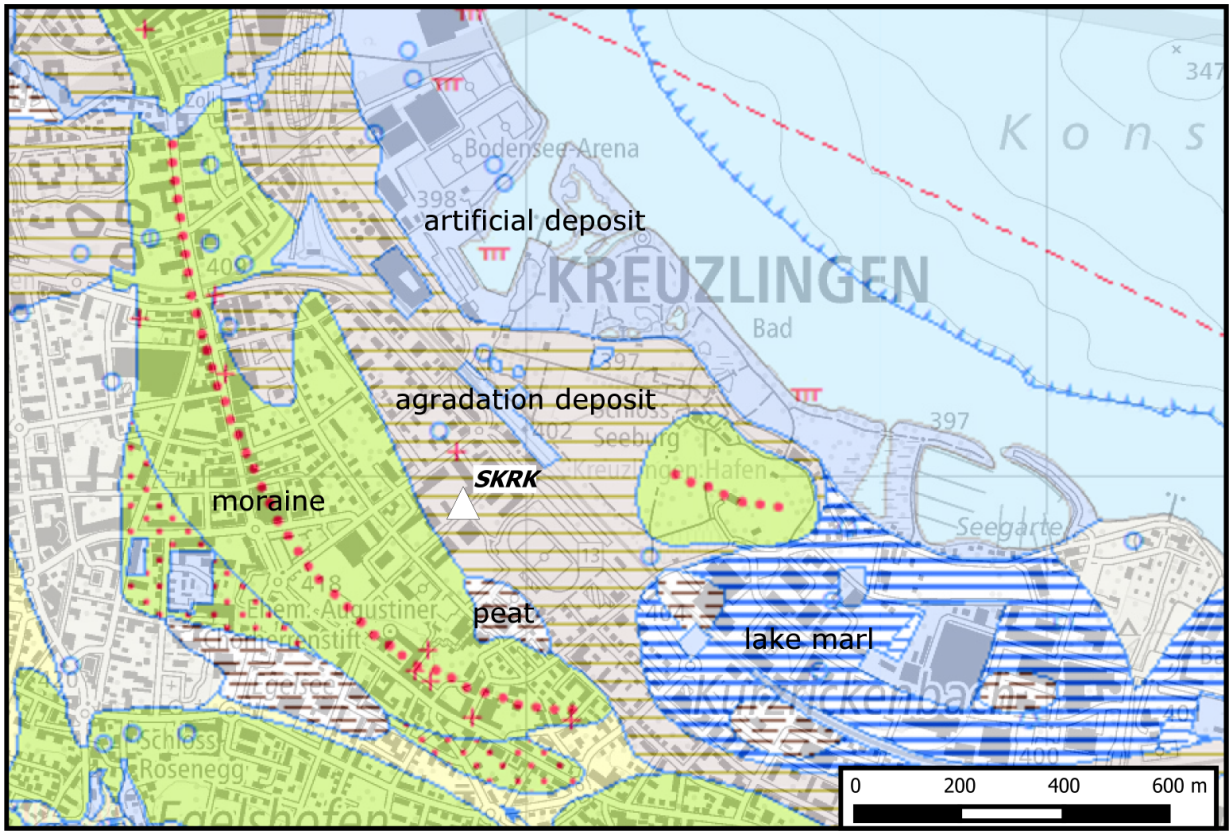

Figure 2: Geological map of the area around station SKRK. According to the geological atlas, station SKRK and most stations of the passive array measurement lie on agradation deposits, some stations of the large array in the southwest on the transition zone to moraine.

3 Site characterization measurements

3.1 Data set

In order to characterize the local underground structure around station SKRK, passive seismic array measurements were carried out on 11 July 2015. The layout of the seismic measurements is shown in Fig. 3.
Two array measurements were performed (see Table 1 for the main characteristics). The first array consisted of 16 stations. It was planned to consist of three rings of five stations each around a central station, which was located close to station SKRK. The ring radii were planned to be 10 m, 20 m and 50 m, respectively. The final minimum and maximum inter-station distances in the array were 9.9 m and 94.5 m, respectively. The names of the stations of the first array are composed of "SKRK" followed by a two-digit number (01 to 12, 23, 24, 30, 32). The seismic stations consisted of Lennartz 3C 5 s sensors connected to Quanterra Q330 digitizers. A total of 12 digitizers were used. Twelve sensors were connected to the A channels of the digitizers and another four sensors were connected to B channels.
The second array consisted of 12 stations. For this array, the five stations located on the third ring of the first array were kept. Another ring of five stations with a radius of around 100 m was placed around these stations. The central station of the first array and another station of the innermost ring were kept for the second array. The minimum and maximum inter-station distances of the second array were 10.1 and 201.5 m, respectively. The station names of the stations added in the second array are composed of "SKRK" and a two-digit number between 52 and 62 (52, 56, 58, 60, 62).
The station locations have been measured by a differential GPS system (Leica Viva GS10) which was set up to measure with a precision better than 5 cm. This precision was achieved for all stations except SKRK06, where the obtained precision was 11.9 cm.

Table 1: List of the passive seismic array measurements in Kreuzlingen.

Array name	Number of sensors	Minimum interstation distance [m]	Maximum interstation distance [m]	Recording time [s]
1	16	9.9	94.5	6180
2	12	10.1	201.5	7200

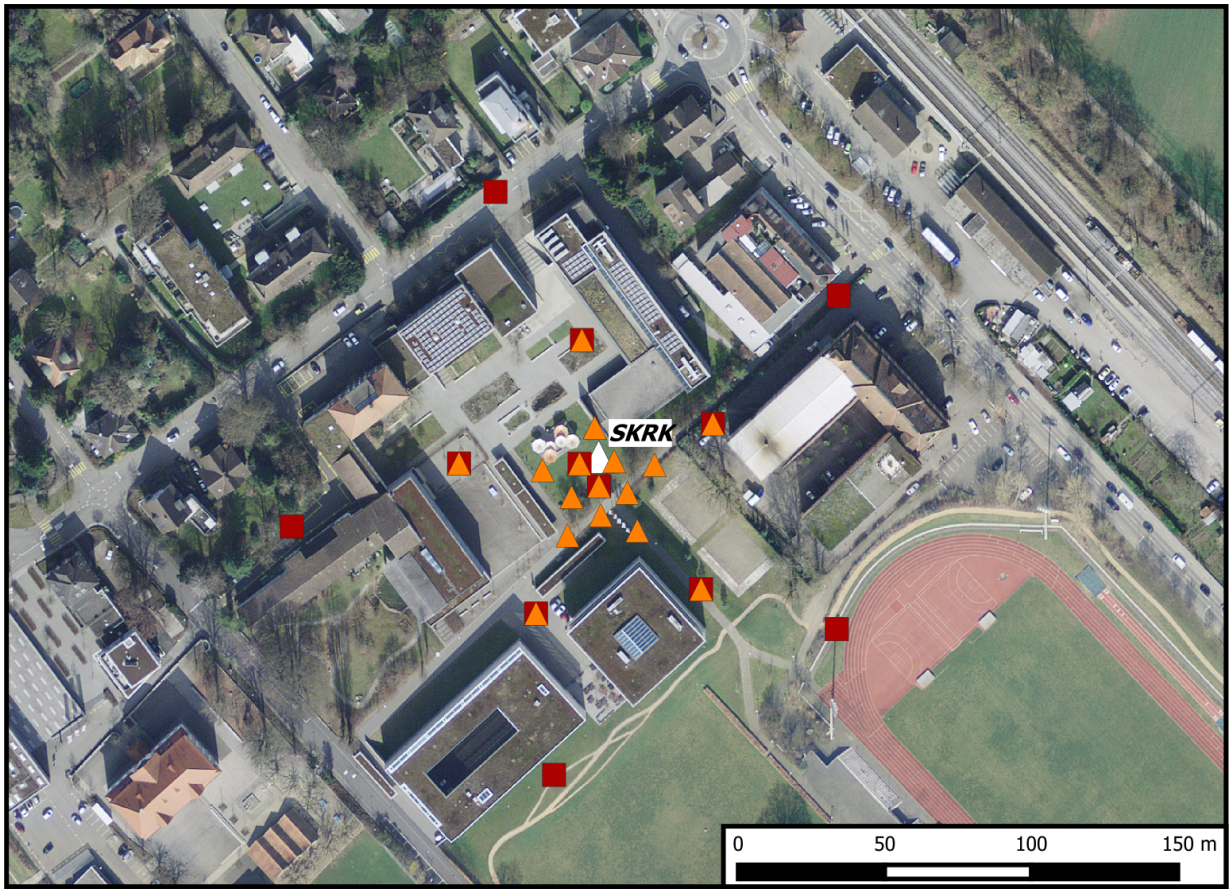

Figure 3: Layout of the array measurements around station SKRK. The location of SKRK is indicated by the white triangle, the locations of the stations for the passive seismic measurement by the orange triangles (first array) and red squares (second array). ©2019 swisstopo (JD100042)

3.2 H/V and RayDec ellipticity curves

Figure 4 shows the H/V curves determined with the time-frequency analysis method (Fäh et al., 2009) for all stations of both passive arrays. All curves are very similar and only show major differences above 5 Hz. The fundamental peak frequency at the different stations varies between 0.49 and 0.63 Hz, the second peak between 2.81 and 3.23 Hz.
The RayDec technique (Hobiger et al., 2009) is supposed to eliminate the contributions of other wave types than Rayleigh waves and give a better estimate of the ellipticity than the classical H/V technique. The RayDec ellipticity curves for all stations of the array measurements are shown in Fig. 4 and are similar to the H/V curves. Station SKRK03, the central station of both arrays, serves as a reference and will be used for the inversion.

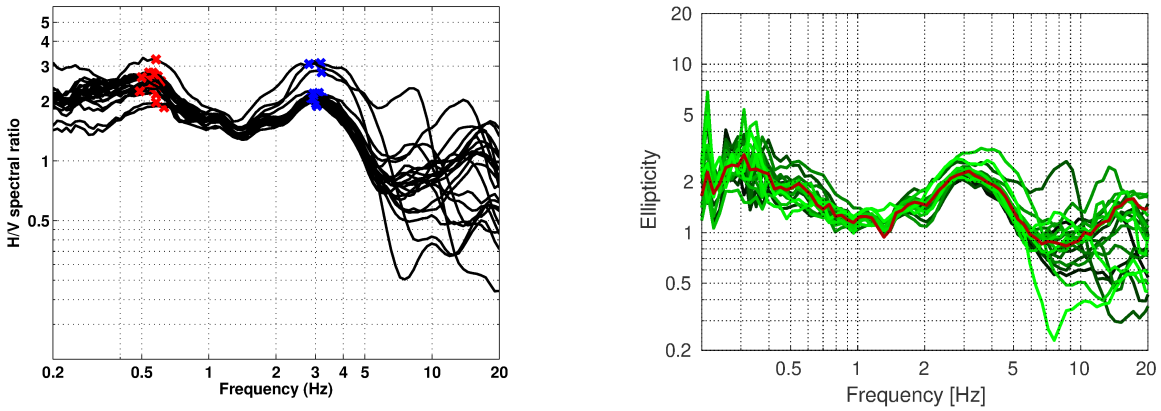

Figure 4: Left: Overview of the H/V measurements for the different stations of both array measurements. Right: RayDec ellipticities for all measurement stations. The red curve corresponds to SKRK03, the central station of both arrays.

3.3 Polarization measurements

The polarization analysis was performed according to Burjánek et al. (2010) and Burjánek et al. (2012). The results for all stations of the array are similar. Only the results for SKRK03, the station in the array center, are shown here.
There is no preferential linear particle polarization visible and we do not see indications for 2-dimensional polarization effects.

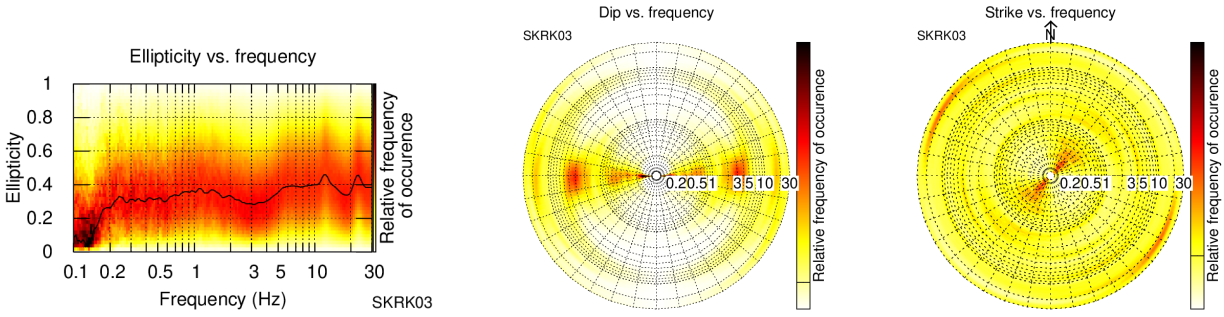

Figure 5: Polarization analysis of station SKRK03.

3.4 3-component high-resolution FK

The results of the 3-component high-resolution FK analysis (Poggi and Fäh, 2010) are shown in Fig. 6 (dispersion curves) and Fig. 7 (ellipticity curves). On the transverse component, corresponding to Love waves, we can clearly identify a dispersion curve for array 1 between 4.4 and 21.9 Hz and for array 2 between 2.6 and 10.2 Hz. The upper-frequency resolution limit of array 1 is not reached, probably because no waves with sufficient energy are present at these frequencies.
On the vertical component, corresponding to Rayleigh waves, we can clearly identify one mode between 5.5 and 25.2 Hz for array 1 and between 3.4 and 10.2 Hz for array 2. On the radial component, also related with Rayleigh waves, the results are less clear, but we can also see dispersion curves for a single mode using each array.
The corresponding ellipticity curves of these modes (Fig. 7) show signs of a peak around 3 Hz and are mostly flat above 5 Hz.

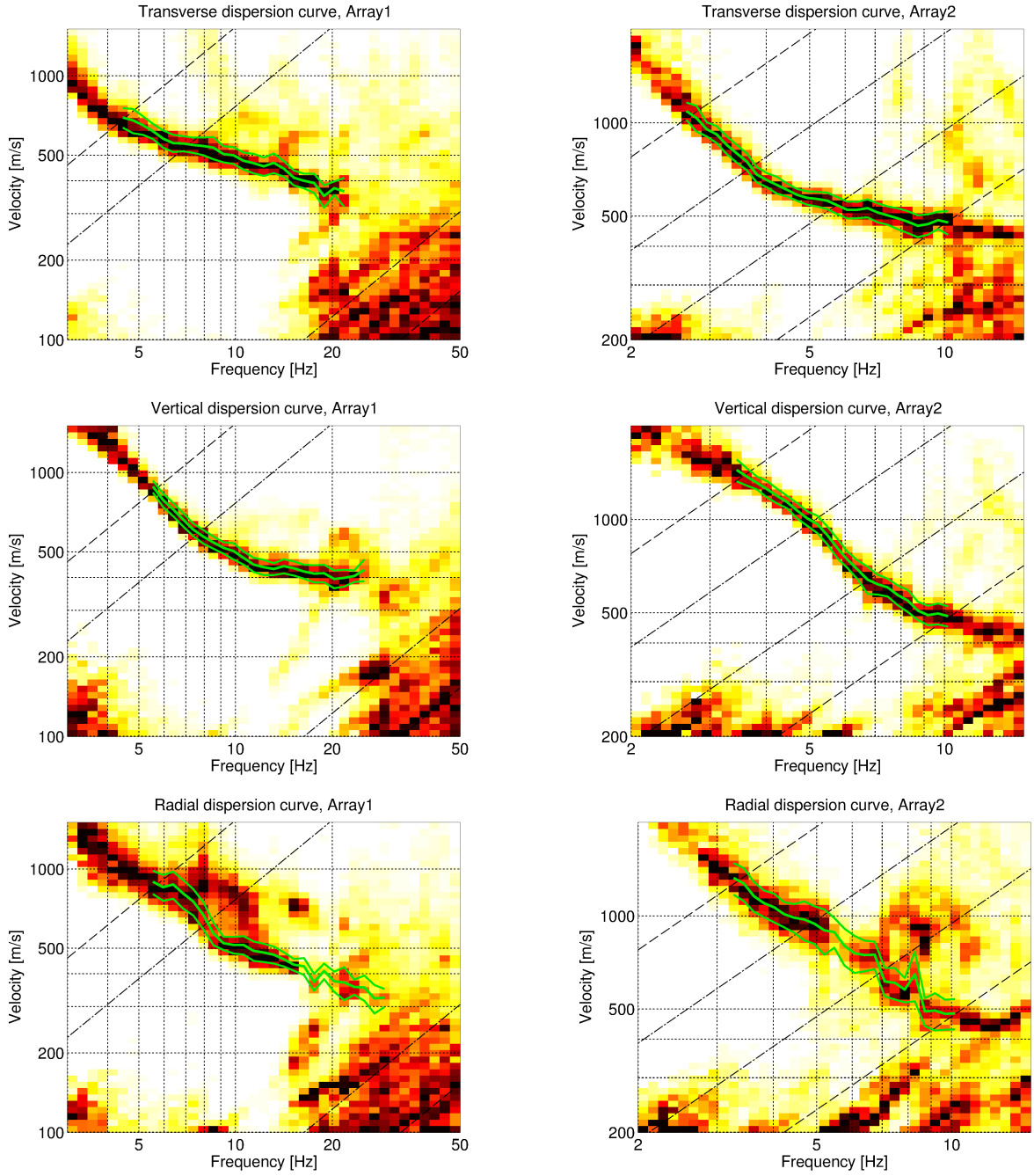

Figure 6: Dispersion curves obtained with the 3-component HRFK algorithm (Poggi and Fäh, 2010). In the left column, the dispersion curves for the transverse, vertical and radial components are shown for array 1, and in the right column for array 2. The dashed and dotted black lines are the array resolution limits. The solid green lines are picked from the data, where the central line indicates the best values and the two outer lines the standard deviation.

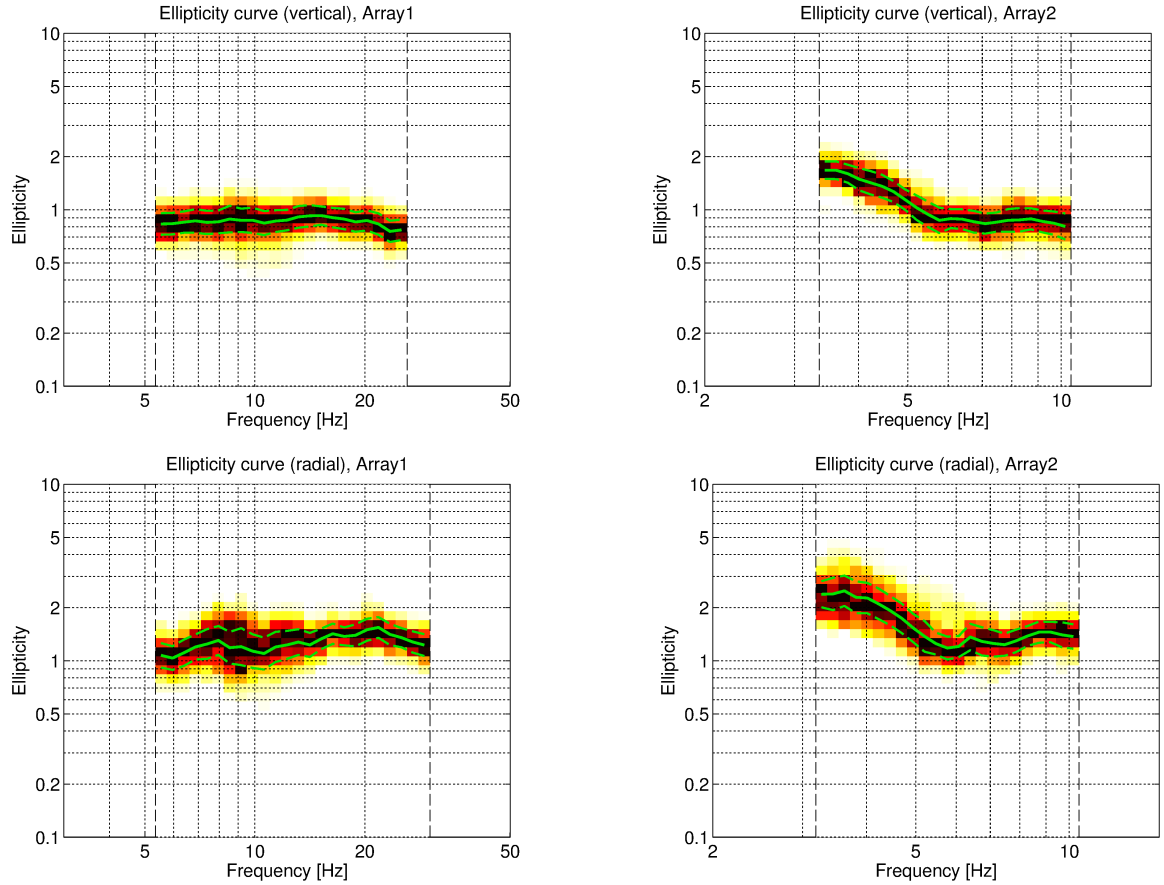

Figure 7: Ellipticity curves obtained with the 3-component HRFK algorithm (Poggi and Fäh, 2010) corresponding to the picked dispersion curves on the vertical and radial components for array 1 (left column) and array 2 (right column). The solid green lines are picked from the data, where the central line indicates the best values and the two outer lines the standard deviation.

3.5 WaveDec

The results of the WaveDec (Maranò et al., 2012) processing are shown in Figs 8 and 9. This technique estimates the properties of single or multiple waves simultaneously with a maximum likelihood approach. In order to improve the results, the parameter γ, which modifies the sharpness of the wave property estimation, has been tuned. Here, a value of $\gamma = 0.2$ was used, corresponding to a predominantly maximum likelihood estimation. The Love wave dispersion curve is clearly identified for array 1 between 3.8 and 19.4 Hz, without reaching the upper-frequency theoretical array resolution limit. For array 2, the curve was picked between 2.6 and 7.0 Hz.
The Rayleigh wave dispersion curve is retrieved between 5.4 and 36.5 Hz for array 1 and, less clear, between 3.6 and 8.0 Hz for array 2. The ellipticity angles for the picked Rayleigh wave dispersion curves are positive below about 5.9 Hz, corresponding to prograde particle motion, and negative, indicating retrograde particle motion, at higher frequencies. There might be another change of the sense of particle motion around 35 Hz, but with a lot of uncertainty.

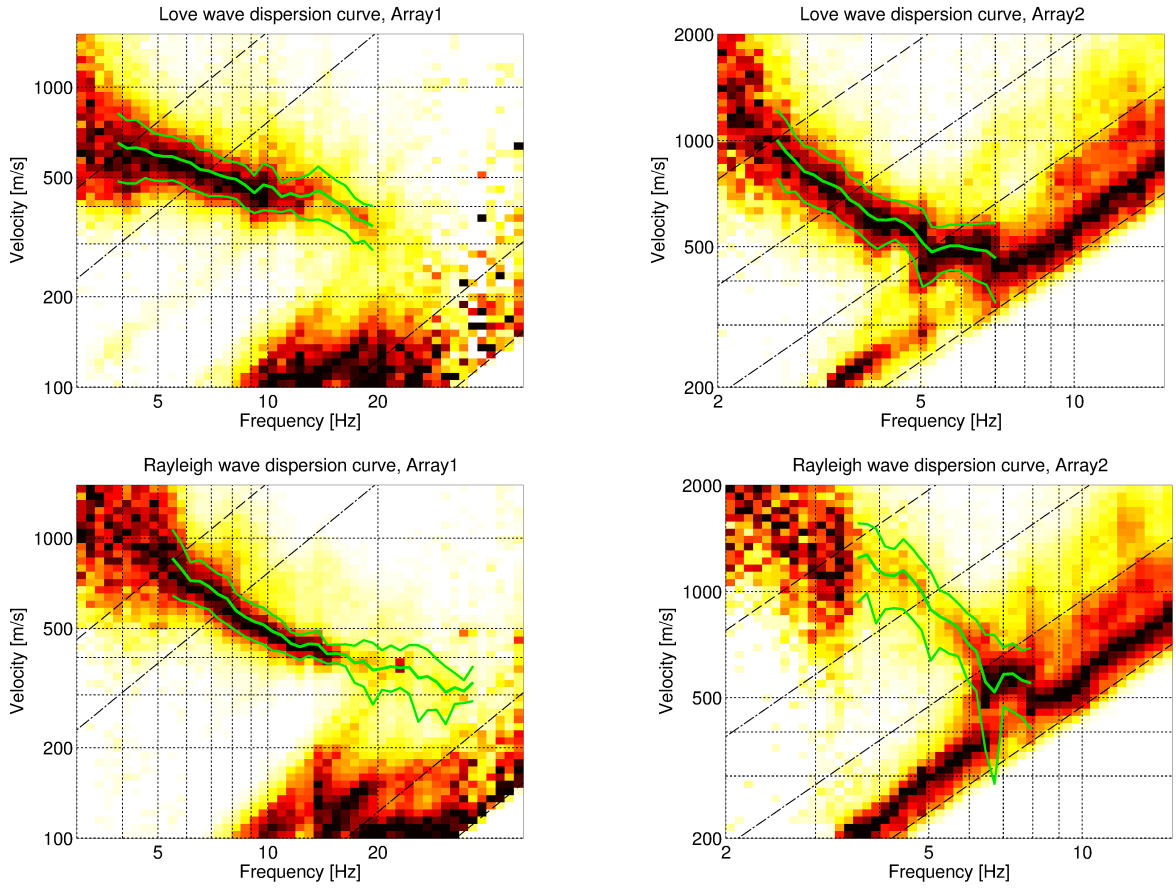

Figure 8: Love (top line) and Rayleigh (bottom line) wave dispersion curves obtained with the WaveDec technique (Maranò et al., 2012) for array 1 (left) and array 2 (right). The dashed lines indicate the theoretical array resolution limits.

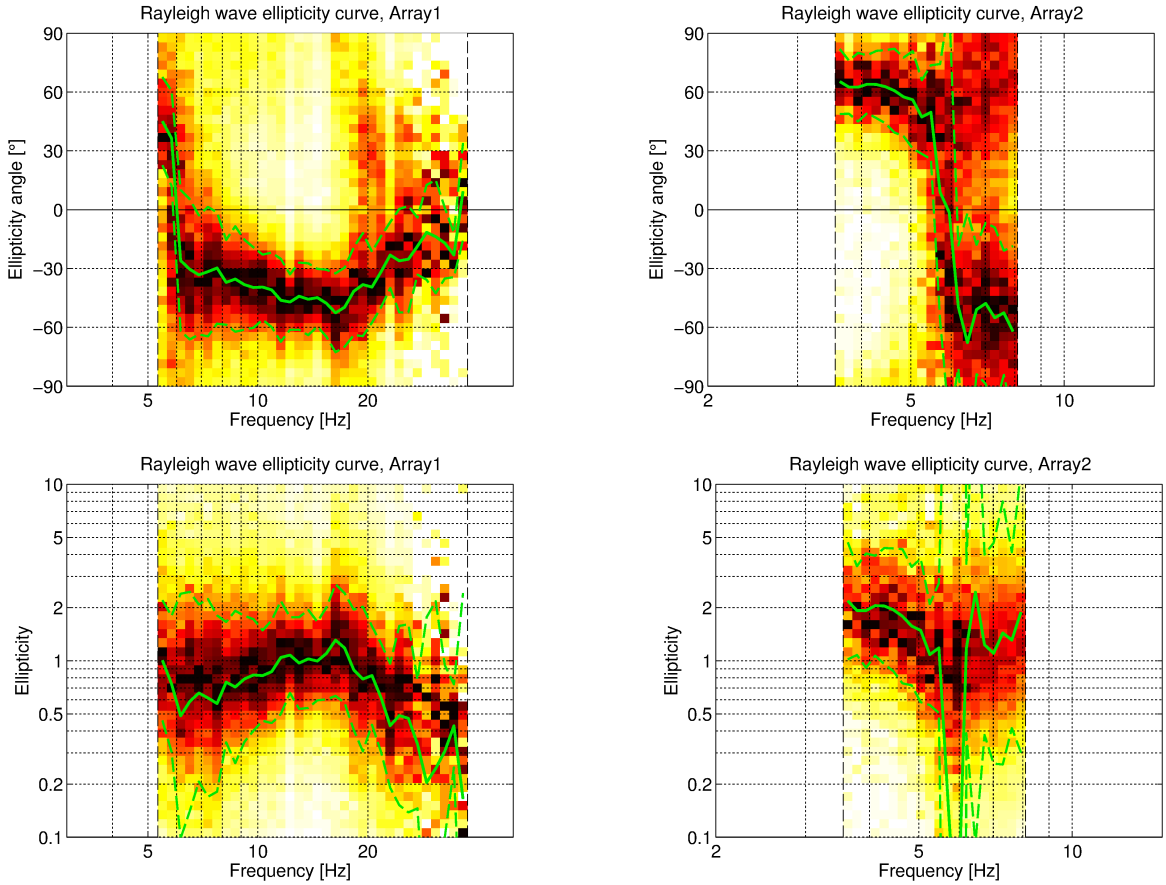

Figure 9: Rayleigh wave ellipticity curves obtained with the WaveDec technique (Maranò et al., 2012). Top line: Rayleigh wave ellipticity angles obtained using array 1 (left) and array 2 (right). Bottom line: Rayleigh wave ellipticity curve, i.e. the absolute value of the tangent of the ellipticity angle, for the curve of array 1 (left) and array 2 (right).

3.6 SPAC

The SPAC (Aki, 1957) curves of the vertical components have been calculated using the M-SPAC (Bettig et al., 2001) technique implemented in geopsy. Rings with different radius ranges had been defined previously and for all station pairs with distance inside this radius range, the cross-correlation was calculated over a wide frequency range. These cross-correlation curves are averaged for all station pairs of the respective ring and give the SPAC curves. The rings are defined in such a way that at least three station pairs contribute and that their connecting vectors have a good directional coverage.
The SPAC curves for all defined rings are shown in Fig. 10 for array 1 and Fig. 11 for array 2. The black points indicate the data values which contributed to the final dispersion curve estimation, which was made with the function `spac2disp` of the geopsy package. These resulting dispersion curves are shown in Fig. 12.
Using SPAC, we can retrieve a Rayleigh wave dispersion curve between 4.4 and 15.9 Hz for array 1 and between 3.5 and 6.8 Hz for array 2.

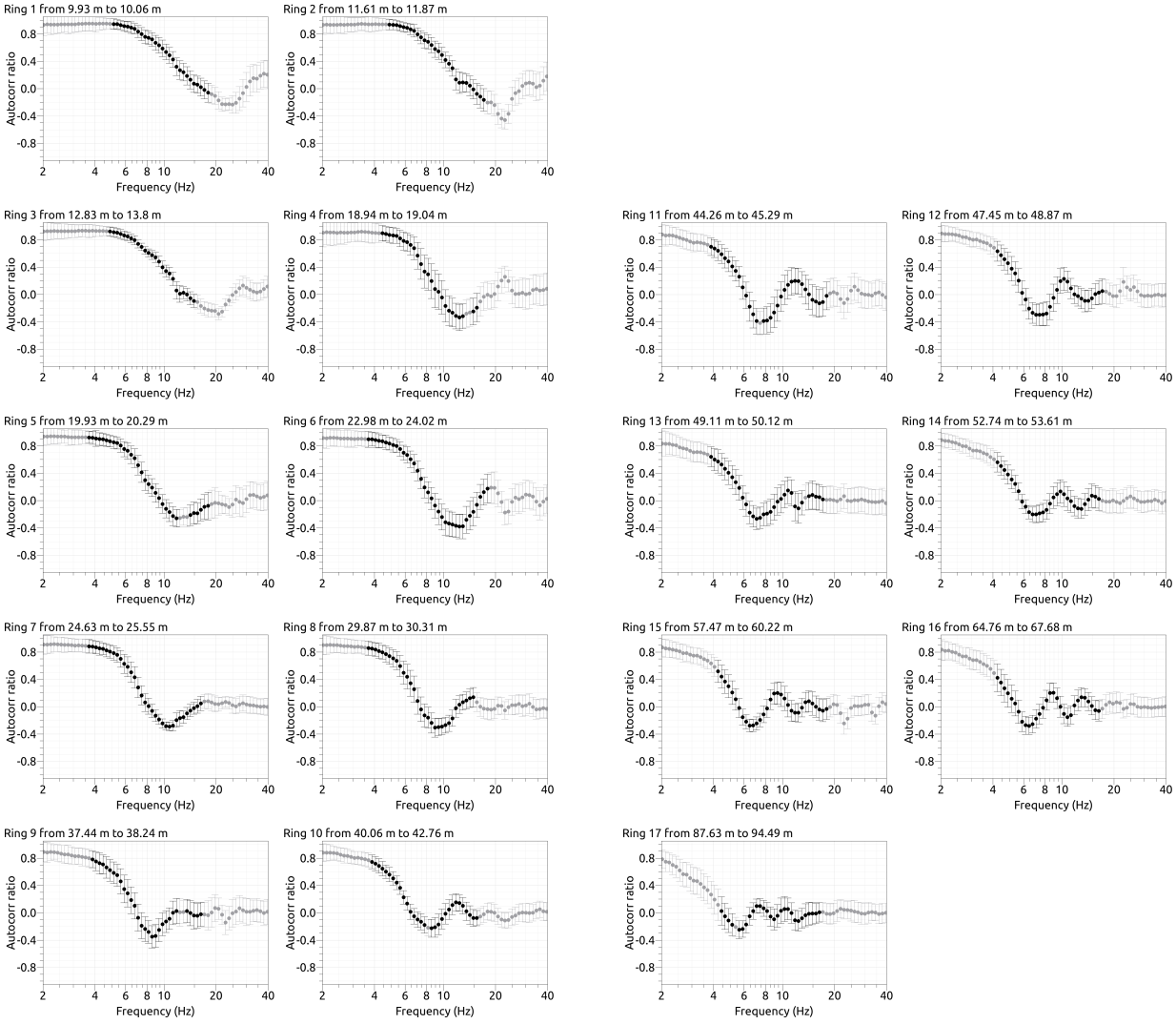

Figure 10: SPAC curves for array 1. The black data points contributed to the dispersion curve estimation.

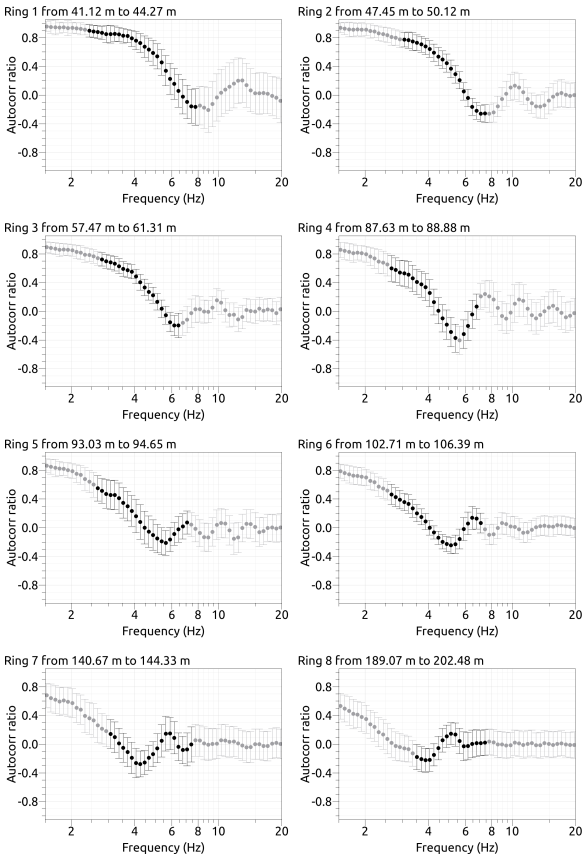

Figure 11: SPAC curves for array 2. The black data points contributed to the dispersion curve estimation.

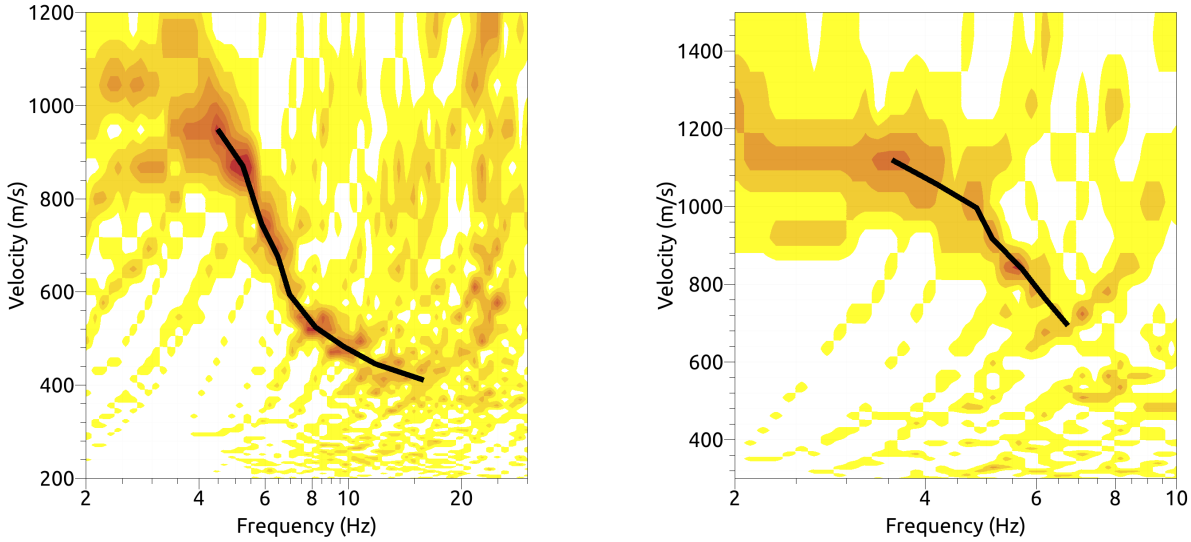

Figure 12: Resulting Rayleigh wave velocities for array 1 (left) and array 2 (right). The black line corresponds to the picked dispersion curve.

3.7 Summary

Fig. 13 gives an overview of the dispersion and ellipticity curves determined by the different methods.
For Love waves, the HRFK and WaveDec results for the respective arrays are in good overall agreement. For both arrays, WaveDec gives systematically lower velocities than HRKF and there are some minor discrepancies between both arrays. Nevertheless, we can identify a continuous dispersion curve between 2.6 and 21.8 Hz. The high-frequency array resolution limit was not reached.
For the Rayleigh waves, there is a very good agreement between the different methods. The radial HRFK curve of array 1 and the WaveDec curve for array 2 show some deviations from the overall trend around 7 Hz. In any case, we can define a continuous dispersion curve from around 3.4 and 36.5 Hz.
The ellipticity curves retrieved using the different methods are in good qualitative agreement. The single-station ellipticity curve determined with RayDec is the only one to cover frequencies lower than 3 Hz. It was transformed to ellipticity angle by using the arctan function. As we cannot distinguish between prograde and retrograde particle motion with a single-station method, we account for both possibilities and the RayDec (and HRFK) curves are represented twice, once for each sense of rotation. In the ellipticity angle representation, the WaveDec curves for both arrays show prograde particle motion below 6 Hz and retrograde particle motion above. Below 6 Hz, they are in good agreement with the RayDec and HRFK curves. Above 6 Hz, there is more discrepancy between the different curves. In any case, the results indicate that the ellipticity peak at around 3 Hz has to correspond to a singularity with retrograde particle motion below and prograde particle motion above and that there is a trough at around 6 Hz, where the particle motion changes back to retrograde. We cannot determine if the low-frequency peak at around 0.6 Hz is also a singularity or not.

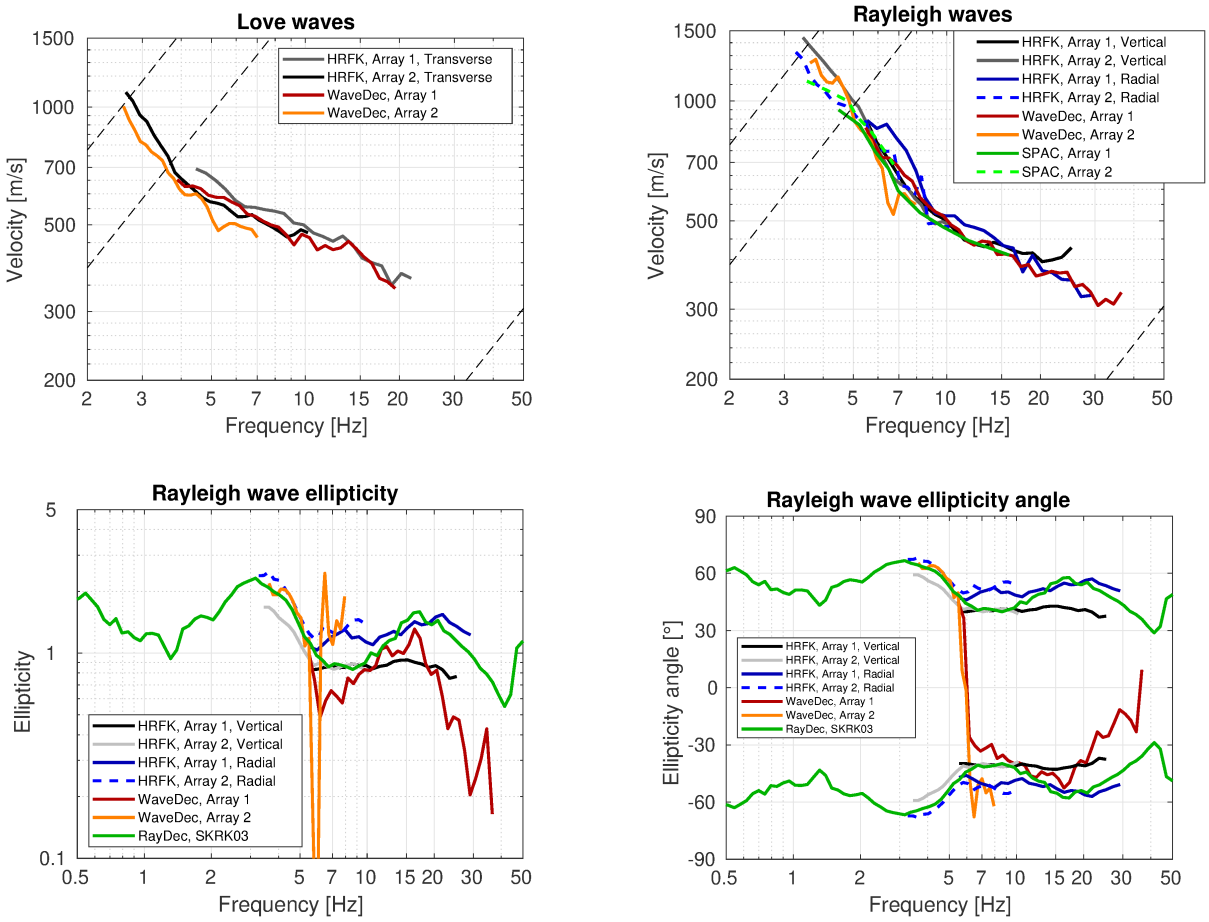

Figure 13: Overview of the Love and Rayleigh wave dispersion curves as well as the ellipticity and ellipticity angle curves for both arrays. The dashed lines indicate the theoretical resolution limits of the array. The RayDec ellipticity curve corresponds to station SKRK03.

4 Data inversion

4.1 Inversion targets

We performed inversions using the Love and Rayleigh wave dispersion curves together with the Rayleigh wave ellipticity angle as inversion targets. For the dispersion curves, a combination of the dispersion curves from HRFK for array 2 and WaveDec for array 1 was used for both Love and Rayleigh waves. For the ellipticity angle, the RayDec curve below the peak at 3 Hz was used, assuming retrograde particle motion, combined with the prograde WaveDec curve for array 2 between the 3 Hz peak and the trough at around 6 Hz and the retrograde WaveDec curve for array 1 above 6 Hz. We did not use the fundamental peak at around 0.5-0.6 Hz for the inversion. The details of the inversion targets are indicated in Table 2 and the corresponding curves are shown in Fig. 14.

4.2 Inversion parameterization

For the inversion, six different parameterizations have been used in total. The first five had free values of the depths and velocities of the different layers, ranging from four to eight layers (including half-space). The last parameterization had fixed layer depths and consisted of 15 layers in total. The main interface depths resulting from the 8-layer inversion were used in the fixed-layer approach. The P-wave velocities were allowed to vary up to 5000 m/s. The S-wave velocities were allowed to range from 50 to 3500 m/s. The deepest layers were parameterized to range to a depth of 200 m maximum. The density was fixed to 2 300 kg/m^3 for the lowest layer, to 1 900 kg/m^3 for the superficial layer (or the first three layers in the fixed-layer case) and to 2 100 kg/m^3 for all other layers. No low-velocity zones were allowed.

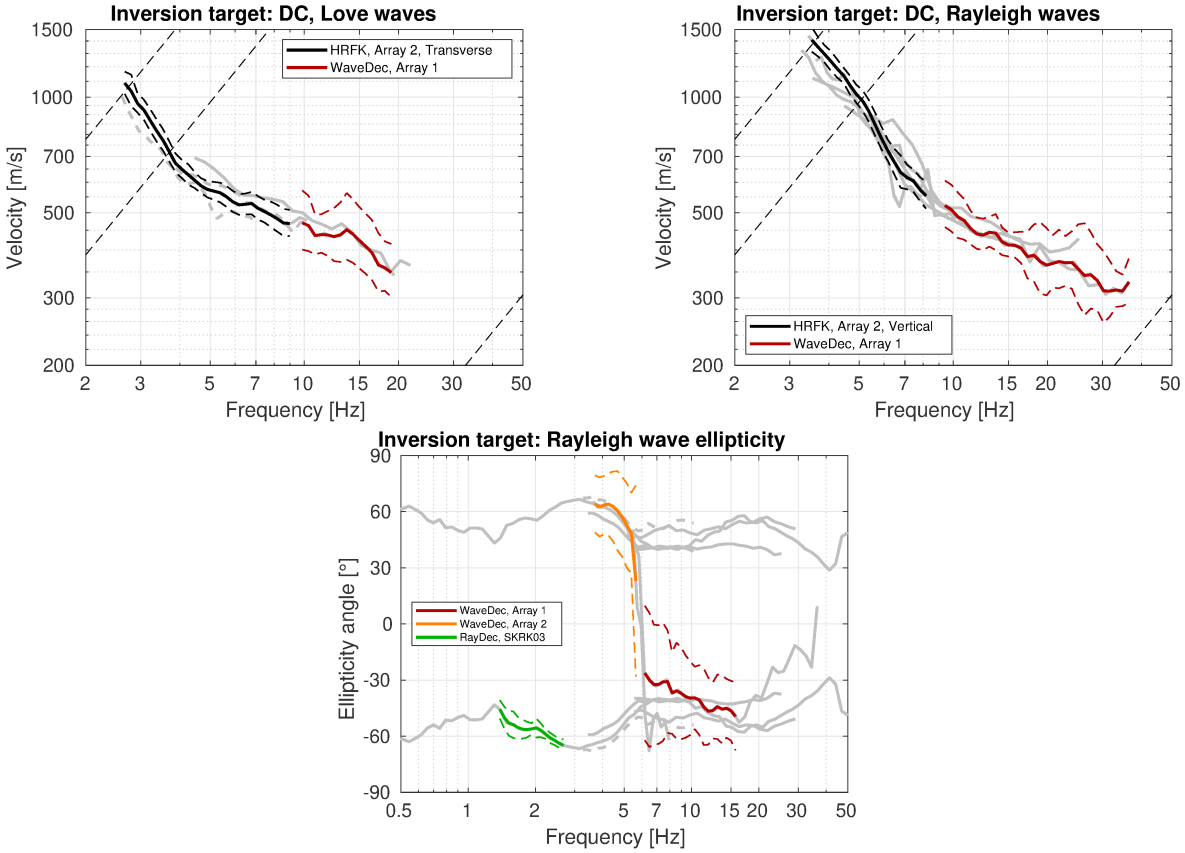

Figure 14: Overview of the dispersion (top) and ellipticity angle (bottom) curves used as targets for the different inversions.

Table 2: List of the different data curves used as target in the different inversions.

Array	Method	Wave type	Mode	Curve type	Frequency range [Hz]
2	HRFK (T)	Love	fundamental	dispersion	2.66 - 8.98
1	WaveDec	Love	fundamental	dispersion	9.85 - 19.0
2	HRFK (V)	Rayleigh	fundamental	dispersion	3.52 - 8.18
1	WaveDec	Rayleigh	fundamental	dispersion	9.40 - 36.5
	RayDec (SKRK03)	Rayleigh	fundamental	ellipticity angle	1.38 - 2.67
2	WaveDec	Rayleigh	fundamental	ellipticity angle	3.69 - 5.63
1	WaveDec	Rayleigh	fundamental	ellipticity angle	6.17 - 15.8

4.3 Inversion results

We performed six inversions with different parameterizations for the different targets. In Table 3, the obtained minimum misfit values for these inversions are shown. Each inversion run produced around 150 000 total models in order to assure a good convergence of the solution, except for the 4-layer inversion, where 100 000 generated models were sufficient. The results of the inversions SKRK4l to SKRKfix are shown in Figs 15 - 20. The different inversions yield similar misfit values and fit the data in a comparable way. The 4-layer and 5-layer inversions yield slightly higher misfit values than the 6-, 7- and 8-layer inversions. Using the fixed-depth approach, the minimum misfit was also higher, probably because the interface depths were fixed at non-optimum depths.

Table 3: List of inversions

Inversion	Number of layers	Number of models	Minimum misfit
SKRK4l	4	100 005	0.469
SKRK5l	5	150 009	0.466
SKRK6l	6	150 006	0.396
SKRK7l	7	149 995	0.400
SKRK8l	8	150 035	0.401
SKRKfix	15	150 046	0.500

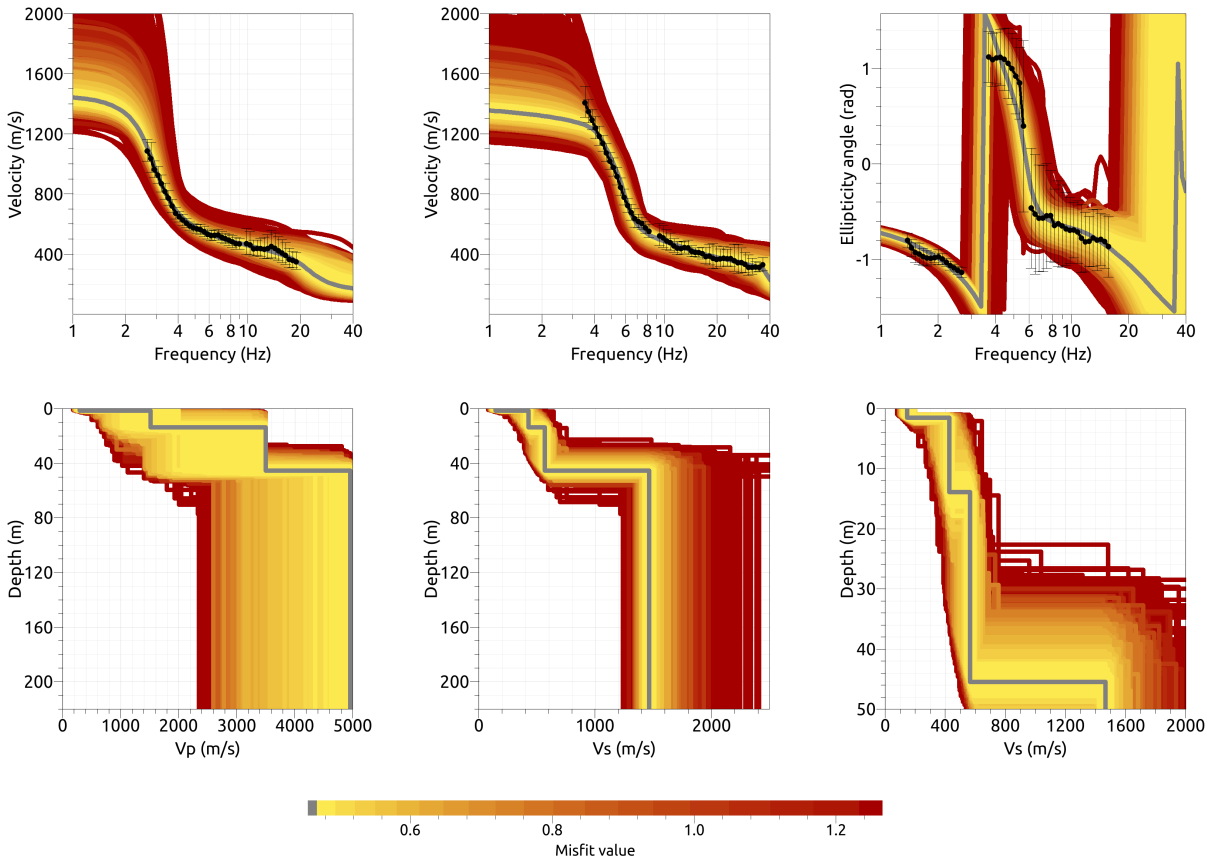

Figure 15: Inversion SKRK4l. Top line: Dispersion curves for Love waves (left) and Rayleigh waves (center) and Rayleigh wave ellipticity curves (right) of the respective fundamental modes. Bottom line: P-wave velocity profiles (left), S-wave velocity profiles (center and zoom on the upper 50 m on the right). The black dots indicate the data points used for the inversion, the gray line indicates the best-fitting model.

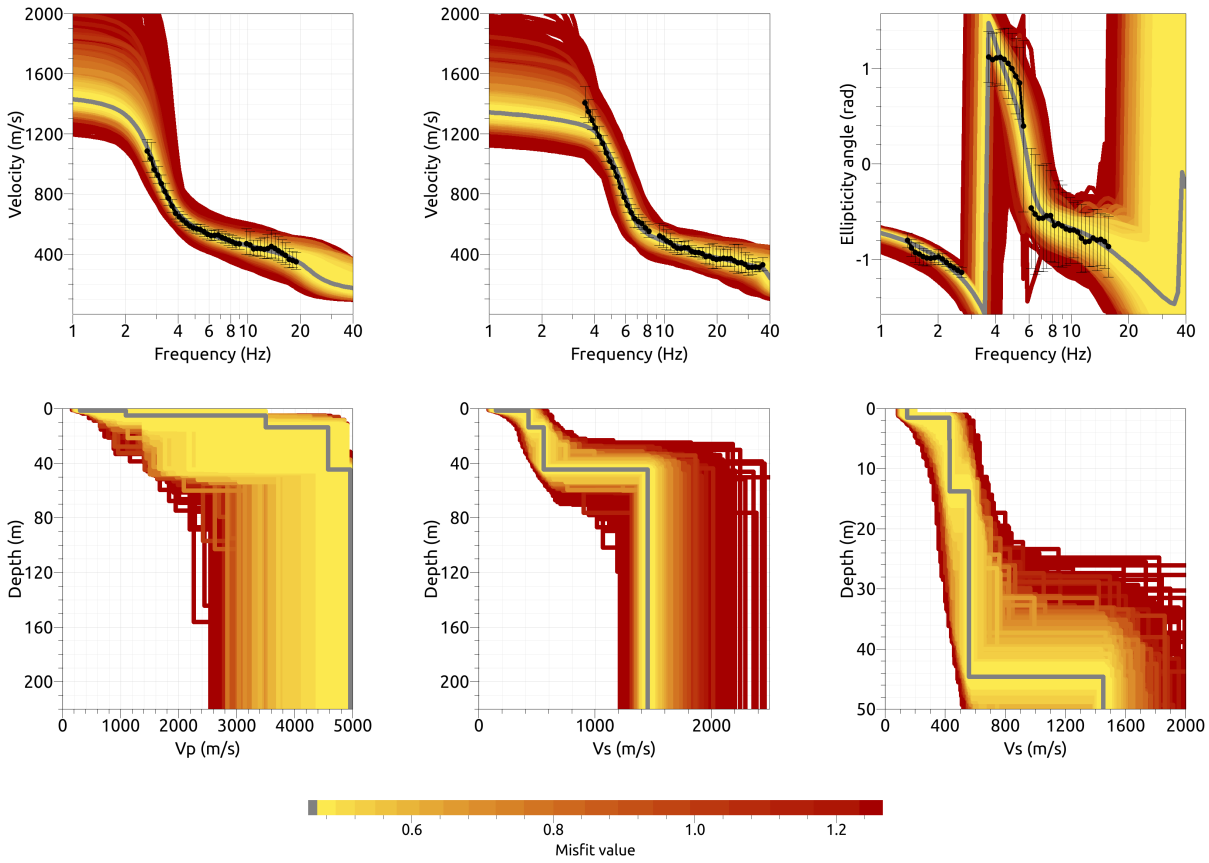

Figure 16: Inversion SKRK5l. Top line: Dispersion curves for Love waves (left) and Rayleigh waves (center) and Rayleigh wave ellipticity curves (right) of the respective fundamental modes. Bottom line: P-wave velocity profiles (left), S-wave velocity profiles (center and zoom on the upper 50 m on the right). The black dots indicate the data points used for the inversion, the gray line indicates the best-fitting model.

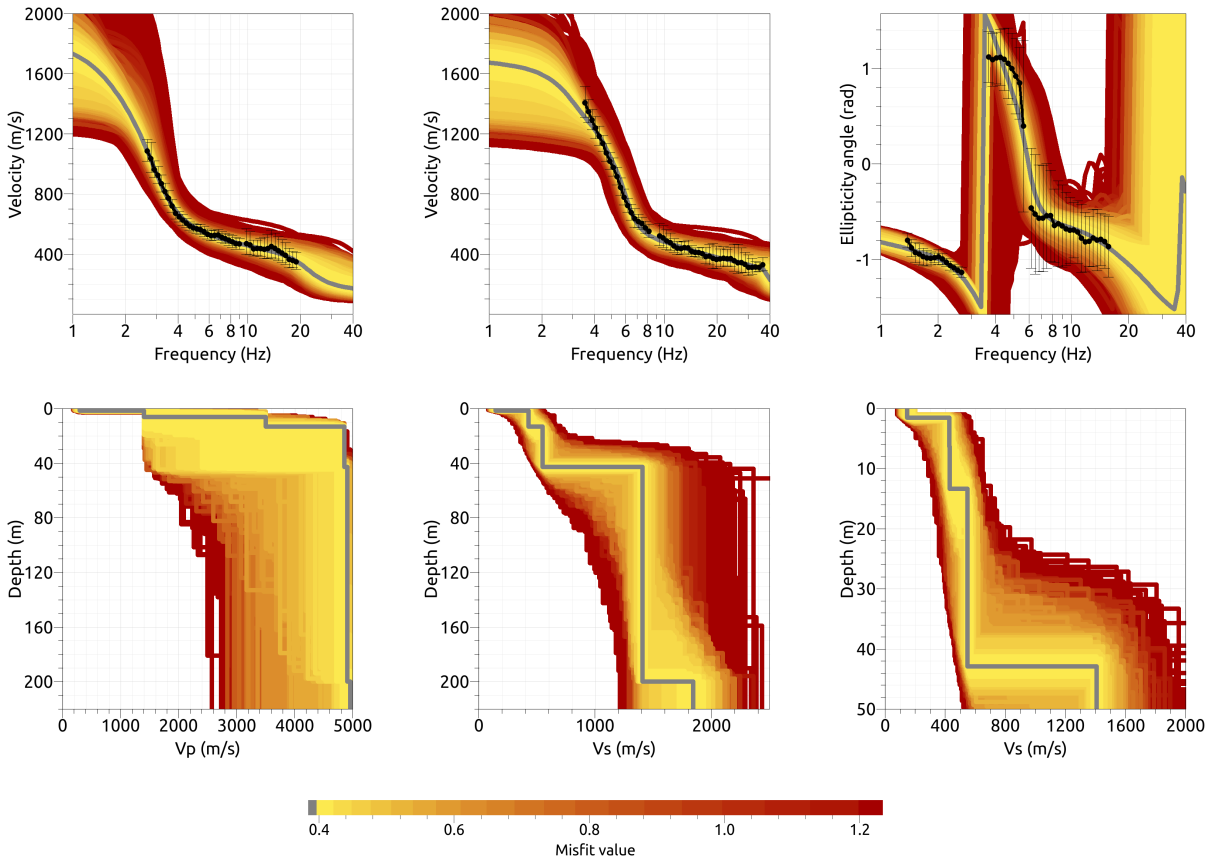

Figure 17: Inversion SKRK6l. Top line: Dispersion curves for Love waves (left) and Rayleigh waves (center) and Rayleigh wave ellipticity curves (right) of the respective fundamental modes. Bottom line: P-wave velocity profiles (left), S-wave velocity profiles (center and zoom on the upper 50 m on the right). The black dots indicate the data points used for the inversion, the gray line indicates the best-fitting model.

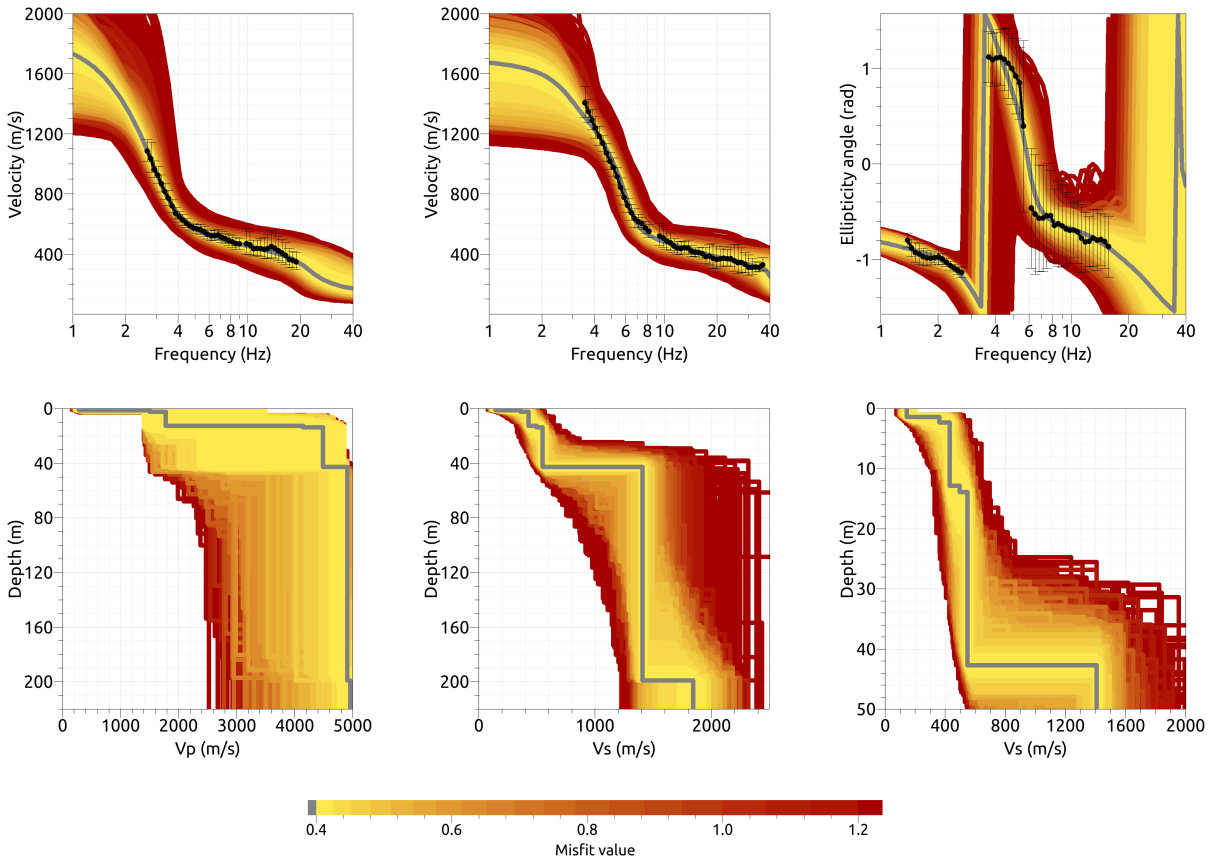

Figure 18: Inversion SKRK7l. Top line: Dispersion curves for Love waves (left) and Rayleigh waves (center) and Rayleigh wave ellipticity curves (right) of the respective fundamental modes. Bottom line: P-wave velocity profiles (left), S-wave velocity profiles (center and zoom on the upper 50 m on the right). The black dots indicate the data points used for the inversion, the gray line indicates the best-fitting model.

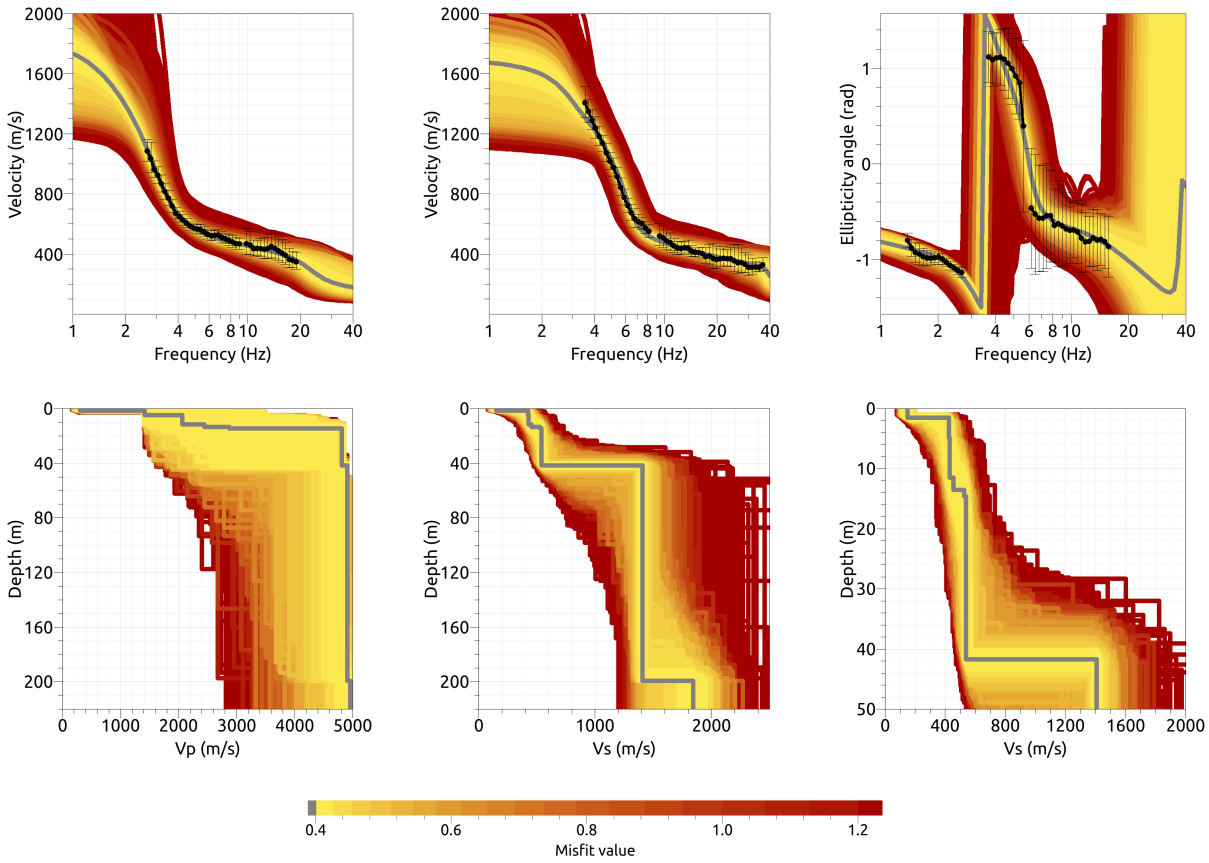

Figure 19: Inversion SKRK8l. Top line: Dispersion curves for Love waves (left) and Rayleigh waves (center) and Rayleigh wave ellipticity curves (right) of the respective fundamental modes. Bottom line: P-wave velocity profiles (left), S-wave velocity profiles (center and zoom on the upper 50 m on the right). The black dots indicate the data points used for the inversion, the gray line indicates the best-fitting model.

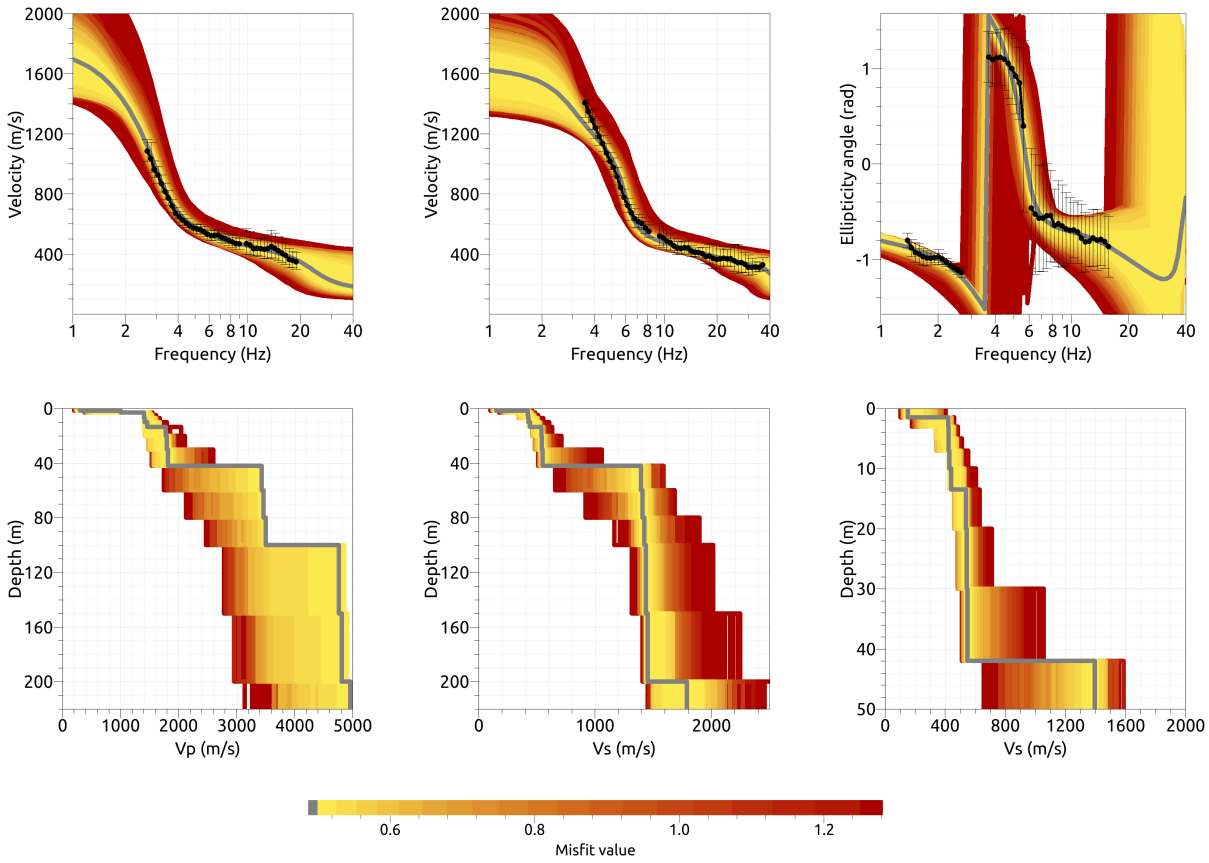

Figure 20: Inversion SKRKfix. Top line: Dispersion curves for Love waves (left) and Rayleigh waves (center) and Rayleigh wave ellipticity curves (right) of the respective fundamental modes. Bottom line: P-wave velocity profiles (left), S-wave velocity profiles (center and zoom on the upper 50 m on the right). The black dots indicate the data points used for the inversion, the gray line indicates the best-fitting model.

4.4 Overview of the inversion result

The best-fitting models of the inversions SKRK4l-SKRKfix are shown in Fig. 21. All models show similar main features. The superficial layer of about 1.5 m depth has a shear-wave velocity of about 150 m/s, followed by a layer with a velocity of about 430 m/s down to about 13.5 to 14 m. The next layer with a velocity of about 550 m/s reaches to about 42 m of depth, where the seismic bedrock with a velocity of over 1400 m/s is found.
The V_{S30} value for the inversions ranges from 434.2 to 439.7 m/s (average value 436.8 $\pm$ 2.1 m/s). This corresponds to soil class B in EC8 and C in SIA261.

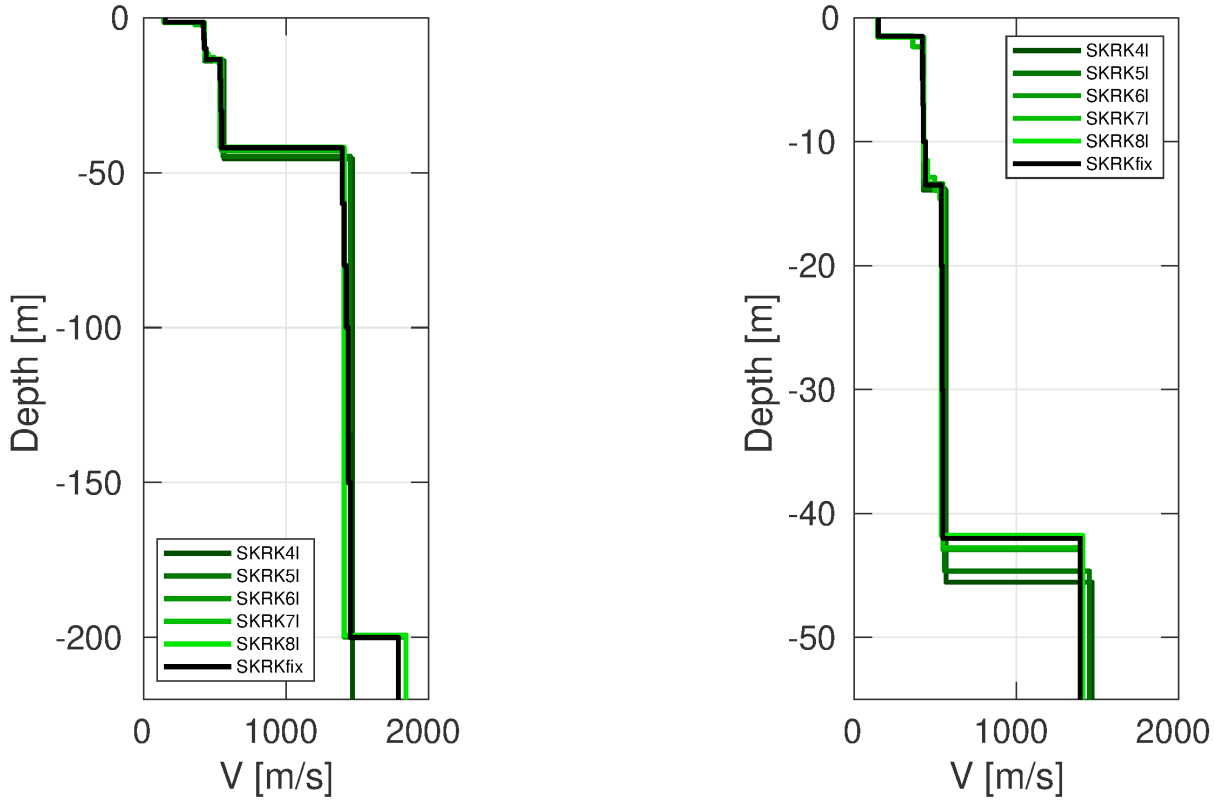

Figure 21: Overview of shear-wave velocity profiles of the best-fitting models of all inversions (left) and a zoom on the shallow part (right).

4.5 Site amplification

In Fig. 22, the theoretical amplification function for the best models resulting from the inversions is compared with the empirical amplification. The empirical amplification for station SKRK is based on 41 events so far. The transfer function for the inversion models is in good agreement with the empirical amplification especially around the peak frequency at 3 Hz. At higher frequencies, the empirical amplification stays at a higher level and has less pronounced peaks and troughs than the modeled amplification. This might be a sign for edge-generated surface waves that impact the site and are not included in the modeling of vertically propagating S-waves. At low frequencies, the empirical amplification shows also a higher level. This might be linked with the observed H/V and ellipticity peak at 0.5 Hz, which was not included in the inversion process.

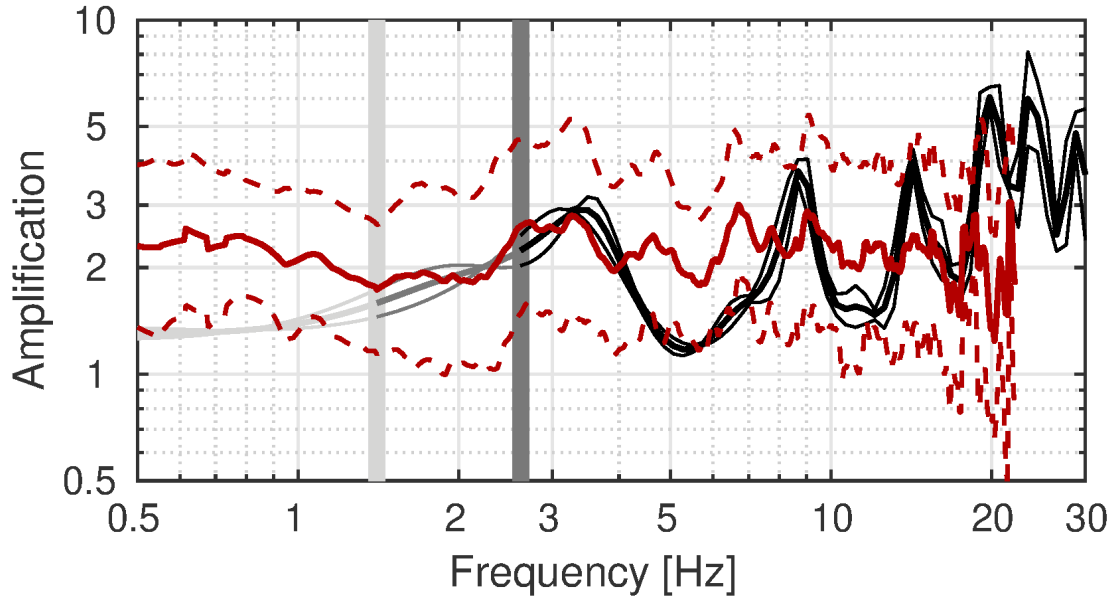

Figure 22: Comparison between the modeled amplification for the final set of best models of the different inversions (SKRK4l-SKRKfix; in grey to black, with standard deviation) and the empirical amplification measured at station SKRK (red, with standard deviation). The vertical light and dark grey bars correspond to the lowest frequency of the ellipticity and dispersion curves, respectively.

4.6 Quarter-wavelength representation

The quarter-wavelength velocity approach (Joyner et al., 1981) provides, for a given frequency, the average velocity at a depth corresponding to 1/4 of the wavelength of interest. It is useful to identify the frequency limits of the experimental data (the minimum frequency of the dispersion curve used in the inversion is 2.66 Hz, the minimum frequency used for the ellipticity inversion 1.38 Hz). The results using this proxy show that the dispersion curves constrain the profiles down to only about 45 m, but the ellipticity information down to about 170 m (Fig. 23). Moreover, the quarter wavelength impedance-contrast introduced by Poggi et al. (2012) is also displayed in the figure. It corresponds to the ratio between two quarter-wavelength average velocities, respectively from the top and the bottom part of the velocity profile, at a given frequency (Poggi et al., 2012). This curve shows a strong contrast at the fundamental frequency of the site.

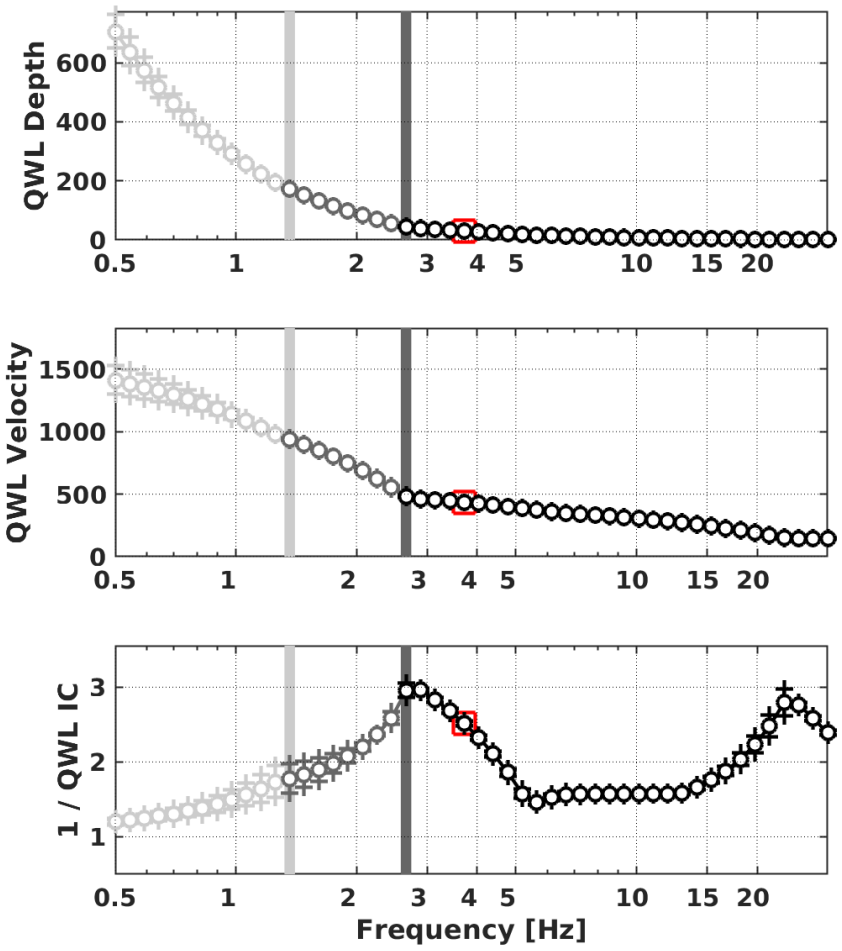

Figure 23: Quarter wavelength representation of the velocity profile for the best models of the inversions (top: depth, center: velocity, bottom: inverse of the impedance contrast). The black curves are constrained by the dispersion curves, the light grey curves are not constrained by the data. The red square corresponds to V_{S30}.

5 Conclusion

We performed a passive array measurement with two arrays to characterize the soil underneath station SKRK in Kreuzlingen (TG), located on agradation deposits of Lake Constance.
The dispersion curves for Love and Rayleigh waves could be measured over a wide frequency range, from around 2.7 to 19 Hz for Love waves and from 3.5 to 36.5 Hz for Rayleigh waves. The fundamental ellipticity peak frequency was measured at around 0.5 to 0.6 Hz, a second, singular peak at around 3 Hz.
The joint inversion of Love and Rayleigh wave dispersion curves and the Rayleigh wave ellipticity angle showed that the structure can be explained by models with interfaces at around 1.5 m, 14 m and 42 m depth. The V_{S30} of the best models is about 437 m/s, corresponding to soil class B in EC8 and C in SIA261.

Acknowledgements

The authors thank Felicitas Stein and Marthe Faber for their help during the array measurements.

References

Aki, K. (1957). Space and time spectra of stationary stochastic waves, with special reference to microtremors. *Bull. Earthquake Res. Inst. Tokyo Univ.*, 35:415–456.

Bettig, B., Bard, P.-Y., Scherbaum, F., Riepl, J., Cotton, F., Cornou, C., and Hatzfeld, D. (2001). Analysis of dense array noise measurements using the modified spatial auto-correlation method (SPAC): application to the Grenoble area. *Boll. Geof. Teor. Appl.*, 42:281–304.

Burjánek, J., Gassner-Stamm, G., Poggi, V., Moore, J. R., and Fäh, D. (2010). Ambient vibration analysis of an unstable mountain slope. *Geophys. J. Int.*, 180:820–828.

Burjánek, J., Moore, J. R., Molina, F. X. Y., and Fäh, D. (2012). Instrumental evidence of normal mode rock slope vibration. *Geophys. J. Int.*, 188:559–569.

Fäh, D., Wathelet, M., Kristekova, M., Havenith, H., Endrun, B., Stamm, G., Poggi, V., Burjanek, J., and Cornou, C. (2009). Using ellipticity information for site characterisation. NERIES deliverable JRA4 D4, available at http://www.neries-eu.org.

Hobiger, M., Bard, P.-Y., Cornou, C., and Le Bihan, N. (2009). Single station determination of Rayleigh wave ellipticity by using the random decrement technique (RayDec). *Geophys. Res. Lett.*, 36.

Joyner, W. B., Warrick, R. E., and Fumal, T. E. (1981). The effect of Quaternary alluvium on strong ground motion in the Coyote Lake, California, earthquake of 1979. *Bull. Seismol. Soc. Am.*, 71(4):1333–1349.

Maranò, S., Reller, C., Loeliger, H.-A., and Fäh, D. (2012). Seismic waves estimation and wavefield decomposition: Application to ambient vibrations. *Geophys. J. Int.*, 191:175–188.

Poggi, V., Edwards, B., and Fäh, D. (2012). Characterizing the Vertical-to-Horizontal ratio of ground motion at soft-sediment sites. *Bull. Seismol. Soc. Am.*, 102(6):2741–2756.

Poggi, V. and Fäh, D. (2010). Estimating Rayleigh wave particle motion from three-component array analysis of ambient vibrations. *Geophys. J. Int.*, 180:251–267.